3D SPHERICAL CONVECTION MODELING OF THE INTERIOR OF CERES. S. D. King[1], M. T. Bland[2], R. Fu[3], R. Park[4], J. Castillo-Rogez[4], C. A. Raymond[4], C. T. Russell[5]. [1]Department of Geoscience, Virginia Tech, Blacksburg, VA (sdk@vt.edu), [2]USGS Astrogeology, Flagstaff AZ, [3]Columbia University, New York, NY, [4]Jet Propulsion Laboratory Pasadena CA, [5]UCLA, Los Angeles CA.

Introduction: Images of Ceres from the Dawn Framing Camera (FC) reveal a heavily cratered surface. Many of these craters appear to be substantially unrelaxed. This is difficult to reconcile with the low density and shape observations available prior to Dawn which suggested that Ceres' interior was differentiated into a rocky core and icy outer shell [e.g., 1, 2].

Based on viscous relaxation modeling the viscosity of water ice is inconsistent with crater depths at Ceres surface temperatures [3]. An increase in viscosity by more than a factor of 100 is needed to maintain the topography of a 100-km diameter crater for 1 Ga [4]. Such a viscosity is also consistent with models of Ceres shape [5]. The presence or absence of near-surface ice has implications for the internal dynamics and thermal evolution of Ceres.

While water ice may be present on Ceres, the outer layer must be composed of more than 50% of a stronger material. This can be illustrated by the relatively simple case of rigid spherical inclusions embedded in an incompressible Newtonian fluid. In this case the 'fluid' matrix represents the ice. The viscosity of a Newtonian fluid with a volume fraction of small rigid spheres, Φ, can be approximated by,

$$\eta = \eta_O \left(1 + 2.5\Phi\right) \quad (1)$$

where η_o is the viscosity of the homogeneous fluid [6,7]. Including the effect of a distribution of inclusion sizes one obtains,

$$\eta = \eta_o \left(1 - \Phi\right)^{-2.5} \quad (2)$$

which approaches Eqn. 1 as Φ becomes small [8]. There is a critical fraction, which depends on the packing of the spheres, at which the incompressible solid spheres prevent any flow from occurring and replaces Φ in Eqn. 2 with Φ/Φ_m where Φ_m is the critical fraction [8]. Applying this to the outer shell assumes that the rock is rigid (relative to the weaker material) and thus can be approximated by rigid spheres. Further assuming the critical fraction Φ_m is 0.64, the value for a random, close packed distribution of nearly spherical objects, results in the curve shown in Fig. 1.

The shape of the curve in Fig. 1 is independent of the reference viscosity. To first order, one could apply Eqn. 2 as a multiplicative factor to any rheological formulation, including rheologies that are a complex function of pressure, temperature, stress and/or grain-size. This is qualitatively consistent with laboratory creep investigations of ice-sand mixtures [e.g., 9].

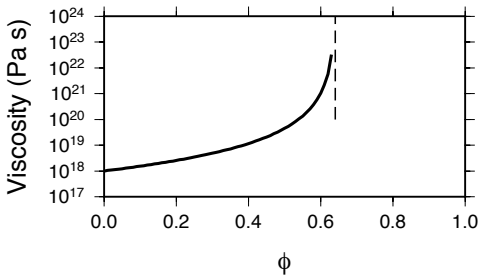

Fig. 1: Eqn. 2 with $\eta_o = 10^{18}$ Pa s and $\Phi_m = 0.64$.

As the fraction of rigid material approaches the critical fraction, the viscosity of the mixture increases exponentially. Thus, near the critical fraction, relatively small changes in the fraction of rigid material will lead to orders of magnitude changes in rheology. If the outer shell is near the critical fraction of rigid material, small changes in the spatial distribution of the rigid material would explain the variability of crater relaxation states seen on Ceres [4].

Geodynamic Modeling: To explore the internal implications of the outer shell on the internal dynamics and thermal evolution of Ceres, we employ 3D spherical thermoviscous flow simulations with a two-layer rheology where the outer shell is based on a 'dirty' ice rheology and the interior is based on a hydrated silicate rheology (e.g., serpentine). For the initial temperature of the interior we assume uniform values of 140 and 180 K with a thin thermal boundary layer at the surface. To avoid problems with the singularity in the equations as the center of the planet, we use a zero heat flux, free-slip inner boundary condition at 0.1 R_p, where R_p is the planet radius. We include radiogenic elements based on carbonaceous chondrite compositions [2] and consider rapid formation cases including heat production from ^{26}Al and ^{60}Fe and as well as late formation cases with no ^{26}Al and ^{60}Fe. The calculations begin with Ceres already differentiated into a hydrated silicate interior, which contains the heat producing elements, surrounded by the weaker outer shell.

Comparison with prior work. The first question is whether the interior of Ceres achieves sub-solidus convection and if so, for how long it remains active. Previous thermal evolution calculations, which considered only thermal diffusion, found that the interior temperature of Ceres rises above the melting point of ice with ^{26}Al decay and even with only long-lived isotopes a substantial portion of the ice within the interior melts [2]. To compare those results with the 3D convection

code, we choose a very large viscosity for both the interior and outer shell such that the calculation never exceeds the threshold for convection. Our radial temperature distribution as a function of time agrees quite well with [2]. Also consistent with [2], the initial temperature has no impact on the overall thermal evolution, as the temperature rises over the first 5 Myr and is controlled by the heat due to the decay of ^{26}Al. Even in case of late formation with no ^{26}Al heating, the heat due to radiogenic decay controls the internal temperature after a relatively short time (<100 Myrs).

The role of convection. With a hydrated silicate interior and a comparatively weaker outer shell, we consider outer shell thicknesses of 47.5 km (R_{shell}=0.9) and 95 km (R_{shell}=0.8). The radiogenic elements are concentrated in the silicate shell as described above. In order to illustrate the time-dependent behavior of the solutions we present the volume-averaged temperature as a function of time in Fig. 2.

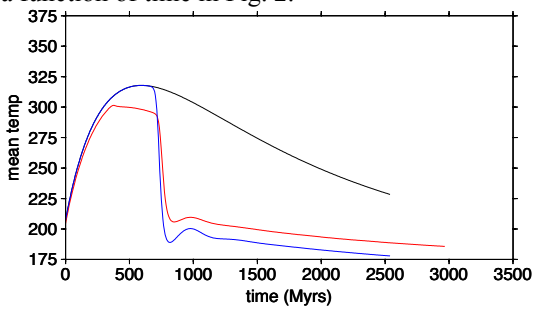

Fig. 2: Volume-averaged temperature as a function of time for a diffusive calculation (black), two-layer structure calculation with a weak outer shell of thickness 47.5 km (blue) and weak outer shell of thickness 95 km (red).

The volume-averaged temperature as a function of time for a diffusive calculation is shown in black for reference. For the first several hundred Myrs of model evolution the blue (47.5-km thick shell) and red (95-km thick shell) average temperatures track the diffusive solution. At approximately 250 Myr, the temperature in the 95-km thick shell (red) calculation levels off and, at approximately 750 Myr there is a dramatic drop in the average temperature. The 47.5-km thick shell (blue) continues to track the diffusive solution until approximately 750 Myr when the average temperature also drops. The temperature in the 95 km thick shell (red) calculation levels off when sub-solidus convection begins in the outer shell (Fig. 3). The 47.5 km thick shell (blue) is too thin to support convection.

In both the 47.5 and 95 km thick outer shell calculations, at 750 Myr the silicate interior becomes convectively unstable and a degree-1 [10] hot hemisphere-cold hemisphere planform develops starting in the inner region (Fig. 4). This structure rapidly removes heat from deep within the body to the surface, cooling the body much faster than by conduction (Fig. 2). This mechanism predicts an asymmetrical surface heat flow and surface age distribution. Although it is predicted to occur in the first Ga of solar system history, the extent to which this mechanism might be consistent with Ceres present-day shape is under investigation.

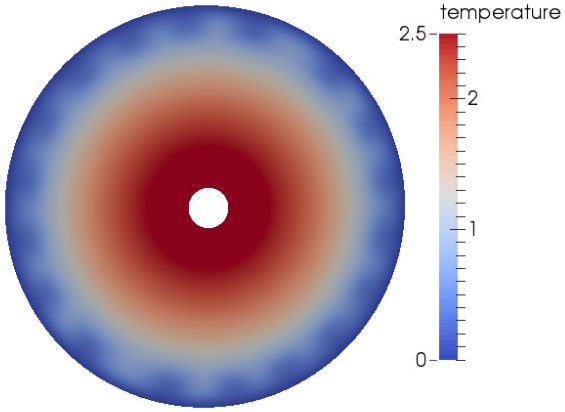

Fig 3. Cross-section through the 95-km thick shell model 250 Myrs after formation showing temperature distribution. The outer shell (blue and white spoke pattern) is convecting. The temperature scale is 130-480 K.

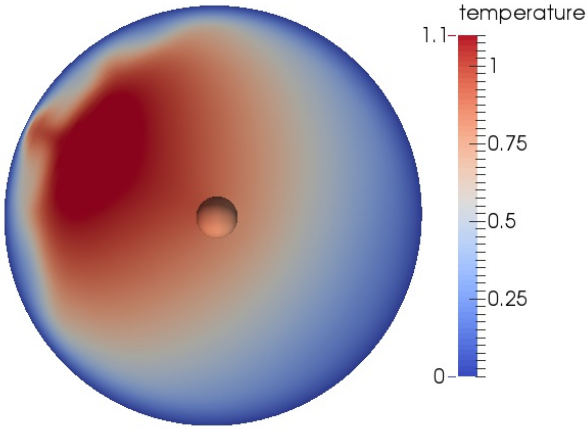

Fig 4. Cross-section through the 95-km thick shell model 750 Myrs after formation showing temperature distribution. The interior has a degree-1 convection pattern. The temperature scale is 130-284 K.

References: [1] Thomas et al. (2005) *Nature* **437,** 224-226. [2] Castillo-Rogez and McCord (2010) *Icarus* **210**, 443-459. [3] Bland (2013) *Icarus* **226**, 510-521. [4] Bland et al. (2016) *This Meeting.* [5] Fu et al. (2015) *AGU Fall Meeting*, P23D-02. [6] Einstein (1906) *Ann. Phys.* **19**, 289-306. [7] Einstein (1911) *Ann. Phys*. **34**, 591-592. [8] Roscoe (1952) *Br. J. Appl. Phys.* **3**, 267-269. [9] Durham et al. (2009) *GRL* **36,** L23203. [10] Roberts and Zhong (2006) *JGR*, **111**, E06013.